PCCP
Physical Chemistry Chemical Physics

Accepted Manuscript

This article can be cited before page numbers have been issued, to do this please use: P. Podupu, A. Ijimakinwa and M. R. Singh, *Phys. Chem. Chem. Phys.*, 2026, DOI: 10.1039/D6CP00296J.

ROYAL SOCIETY OF CHEMISTRY

rsc.li/pccp

View Article Online
DOI: 10.1039/D6CP00296J

Molecular Theory of Oiling-out during Crystallization

Prem K. Reddy[1], Anuoluwaposimi Ijimakinwa[1], and Meenesh R. Singh[1]

[1]Department of Chemical Engineering, University of Illinois Chicago, Chicago, IL 60607

Corresponding Author:

Prof. Meenesh R. Singh
Professor
Department of Chemical Engineering
929 W. Taylor St.
University of Illinois Chicago
Chicago, IL 60607
Tel: (312) 413-7673
Email: mrsingh@uic.edu

Keywords: Oiling-out, Crystallization, Molecular Dynamics, Partial Desolvation, Nucleation

View Article Online
DOI: 10.1039/D6CP00296J

Abstract

Oiling-out, an undesirable liquid–liquid phase separation (LLPS) frequently encountered in pharmaceutical crystallization, poses significant challenges by reducing purity, yield, and process robustness. While macroscopic thermodynamics describes the phase boundaries of oiling-out, the molecular origins of this phenomenon remain poorly understood, with no clear mechanistic framework to explain how solution chemistry triggers phase separation. In this work, we employ atomistic molecular dynamics (MD) simulations to elucidate the molecular mechanism of crystallization during oiling-out in the β-alanine-water-isopropanol (IPA) system. Analysis of radial and spatial distribution functions reveals that LLPS is not driven by the direct replacement of solvent by antisolvent, but by the antisolvent-induced disruption of the hydration network. This breakdown creates solvation voids, regions of incomplete solvation where IPA fails to compensate for the loss of water, resulting in a partially desolvated state that promotes solute clustering. Using a double-well potential analysis, we construct energy landscapes that quantify the activation barriers for crystallization. We identify two distinct kinetic bottlenecks: the enthalpic cost of desolvation and the energetic penalty of structural reorganization. Our results demonstrate that conditions leading to oiling-out drastically lower both barriers compared to homogeneous solutions, reducing the desolvation penalty significantly. These findings confirm that the solute-rich droplets formed during oiling-out serve as kinetically favored precursors, supporting the two-step nucleation theory and providing a quantitative molecular framework for controlling crystallization outcomes in complex solvent mixtures.

View Article Online
DOI: 10.1039/D6CP00296J

Introduction

Crystallization is a cornerstone of chemical and pharmaceutical manufacturing. Solution-based routes frequently encounter oiling-out, also known as liquid–liquid phase separation (LLPS), where a solute-rich liquid separates before crystalline solids form.[1] This phenomenon complicates impurity rejection and particle control, as droplets can trap impurities or disrupt uniform nucleation.[2] At the same time, oiling-out offers unique opportunities: dense liquid droplets often act as precursors that concentrate solute, alter local solvent environments, and reshape nucleation barriers, ultimately steering the kinetics and pathways of crystallization.[3] A clear molecular-level understanding of this mechanism is therefore critical, both to mitigate undesirable effects and to exploit LLPS as a controllable intermediate in crystallization design.

The prevailing framework for understanding crystallization has been rooted in thermodynamics, where the driving force is described in terms of changes in chemical potential, which is often related to the supersaturation.[4] Classical nucleation theory and its extensions treat LLPS as a manifestation of the free-energy landscape, with solute-rich droplets corresponding to metastable minima that compete with direct crystal nucleation.[4, 5] Phase-diagram studies in ternary solvent systems have mapped solubility boundaries, metastable zones, and binodal curves, offering a macroscopic picture of when oiling-out occurs.[6, 7] Complementary analyses have attributed LLPS to shifts in partial molar volumes, solvent activity coefficients, or unfavorable solvation enthalpies, which destabilize homogeneous solutions and promote separation into solute-rich and solute-lean phases.[8-10] While these approaches provide valuable descriptors of phase stability, they abstract away the molecular events of solute-solvent competition and desolvation inside droplets, leaving unanswered how phase separation ultimately facilitates or obstructs crystallization.

Experimental probes such as turbidity/optical microscopy, in situ Raman/IR, and microfluidic solvent-exchange have mapped when LLPS appears, how droplets grow/coalesce, and whether they eventually crystallize, but they resolve structure only at mesoscopic scales and thus remain largely phenomenological with respect to the molecular events that link droplet formation to ordering.[6, 11-13] By contrast, theory and simulation have established that many systems crystallize via two-step pathways, wherein dense-liquid precursors form first and crystalline order then emerges within them; this has been demonstrated with classical DFT and rare-event simulations and is now reviewed as a general motif across small molecules and proteins.[14-16] Atomistic molecular dynamics (MD) studies have further clarified solvent effects on nucleation by quantifying solute-solvent structuring and growth-unit attachment at crystal interfaces, often using enhanced sampling (e.g., umbrella sampling, metadynamics, forward-flux) and carefully chosen order parameters.[16-21] Yet, most computational efforts either target direct crystal nucleation in homogeneous solution rather than oiling-out clusters or depend sensitively on collective variables that may not capture solvation-shell competition inside LLPS

View Article Online
DOI: 10.1039/D6CP00296J

environments. Recent work showed that extracting solvation-shell reorganization and desolvation barriers from MD can yield activation energies, an approach validated for cooling and antisolvent crystallization, but it has not been adapted systematically to oiling-out.[22, 23]

In this work, we address these gaps by developing a molecular-level framework for oiling-out crystallization using the β-alanine-water-isopropanol (IPA) system as a model. Through atomistic MD simulations, we quantify how solute-solvent interactions, solvation-shell occupancy, and desolvation energetics are affected during oiling-out, thereby establishing the microscopic steps that connect molecular rearrangement to crystal growth. Specifically, we (i) analyze radial and spatial distribution functions to resolve the composition of the first solvation shell across solvent environments relevant to oiling-out, (ii) compute binding energies and desolvation barriers that capture solvent reorganization, and (iii) link these energetics to activation barriers for oiling out and crystal growth. Building on prior approaches validated for antisolvent crystallization, we adapt the methodology to LLPS environments, enabling us to propose a general mechanistic model during oiling-out crystallization.[22] The manuscript outlines the molecular simulation methods and analysis workflow; presents results on solvation dynamics, desolvation energetics, and activation barriers; discusses the implications for crystallization pathways; and summarizes the key conclusions and broader significance. A brief overview of the antisolvent and oiling-out crystallization mechanisms is shown in **Figure 1a** and ternary phase diagram of the β-alanine-water-IPA system is shown in **Figure 1b**.

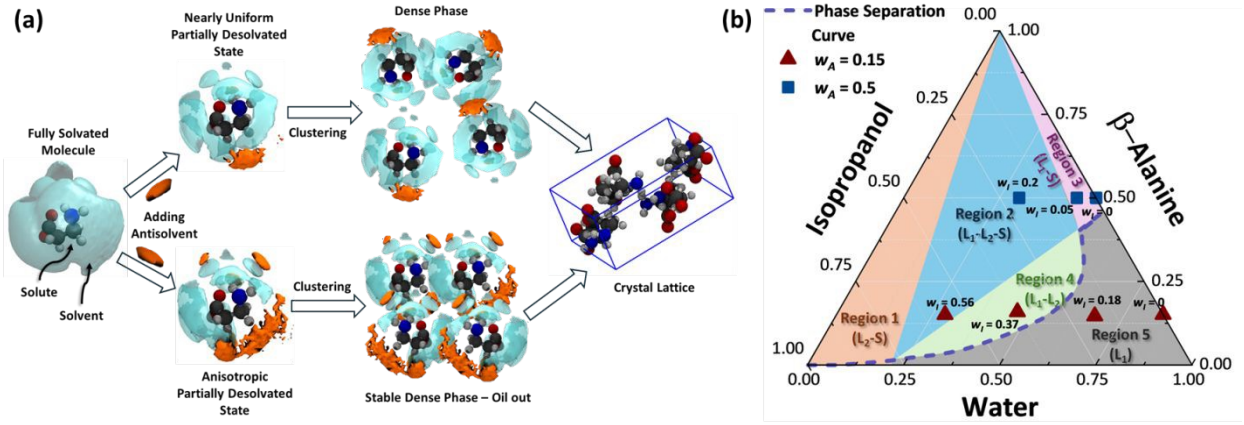

Figure 1: (a) Mechanism of antisolvent crystallization (top) compared with crystallization during oiling-out. β-Alanine (solute) molecules are initially equilibrated in a fully solvated state surrounded by water (solvent) molecules. When IPA (antisolvent) is added, the hydration shell is destabilized and solute molecules move closer, removing excess solvent and antisolvent molecules, resulting in a partially desolvated state. All such partially desolvated states come together to form a dense phase, which are stable during oiling-out. Dense phases lower the energetic barrier for solute-solute reorganization and association, ultimately leading to crystal lattice formation or integration into an existing lattice. (b) Ternary phase diagram of the β-alanine-water-IPA system with concentrations in weight fractions. The purple dashed line is the phase separation curve, and data points shown as red triangles have a solute weight

View Article Online
DOI: 10.1039/D6CP00296J

fraction (w_A) of 0.15, while blue squared points have a solute weight fraction of 0.5. Crystallization is observed in regions 1, 2, and 3, whereas LLPS is observed in regions 2 and 4. L_1 and L_2 refer to two different liquid phases, and S represents a solid phase.

Theoretical Methods

MD simulations were performed using the GROMACS package to investigate the solvation environment of β-alanine (BAL) in water-isopropanol (IPA) mixtures.[24] Cubic simulation boxes of 6 nm (216 nm^3 volume) were constructed at different solvent compositions selected from the ternary β-alanine-water-IPA phase diagram (**Figure 1b)** based on our previous work.[6] Regions 1, 2, and 3 in the phase diagram are where crystallization is observed, with region 1 being IPA-rich, region 3 being water-rich, and region 2 displays LLPS (L_1-L_2-S).[7] On the other hand, regions 4 and 5 show no crystals, but LLPS is observed in region 4 (L_1-L_2). Note that L_1 and L_2 correspond to different phases of liquid, while S denotes the solid phase. Points were chosen to span both the homogeneous (non-LLPS) region and the LLPS regime, as shown in **Figure 1b**, in order to directly compare solute-solvent interactions across phase boundaries. Each system contained BAL molecules at experimentally relevant concentrations, along with explicit water and IPA molecules. The systems were simulated using the Optimized Potential for Liquid Simulations All-Atom (OPLS-AA) force field for a 5 ns production run with a 2 fs time step. More details can be found in Section 1 of the Supporting Information. Radial distribution functions (RDFs) were calculated to characterize the organization of water and IPA molecules around BAL as a whole and around its functional groups (with particular emphasis on the carboxylate and amine moieties). The average coordination numbers were obtained by integrating the RDFs up to the first minimum after the first peak (**Table S2**). Spatial distribution functions (SDFs) were generated using the TRAVIS package, providing three-dimensional density maps of water and IPA around BAL.[25] Comparisons of peak versus bulk densities were used to quantify the extent of solvent enrichment or depletion within the first solvation shell under LLPS and non-LLPS conditions.

Results and Discussion

The RDFs provide a molecular-level insight into the solvation environment of BAL under varying water-IPA compositions, including conditions that span into the LLPS regime. RDFs are especially useful for distinguishing how different solvent components populate the first coordination shell versus the bulk, thereby clarifying interactions and disruptions in the solvation shell and their correspondence to different regions in the ternary phase diagram. The RDFs of water around BAL molecules, shown in **Figure 2**, exhibit a sharp and intense first peak near 0.37 nm, corresponding to strong interactions between water molecules and BAL. This is followed by a distinct minimum and a weaker second peak around 0.5 – 0.6 nm, reflecting structured hydration layers beyond the first shell. At a constant weight fraction of BAL (w_A = 0.15), as the weight fraction of IPA increases, the height of the first peak systematically increases, while the

View Article Online
DOI: 10.1039/D6CP00296J

position remains largely unchanged, as shown in **Figure 2a**. Despite the reduction in bulk water concentration upon IPA addition, the local water density within the first solvation shell remains disproportionately high. This indicates a strong preferential solvation of BAL by water. However, the breakdown of long-range order (diminished second- and third-order peaks) indicates that, while the primary shell is intact, the extended hydrogen-bond network required to stabilize the monomeric state is disrupted by the antisolvent. It is worth noting that, when the number density RDFs of water are plotted, the peak intensity decreases with increasing IPA concentration, as shown in **Figure S1** of the supplementary information. Additionally, the third peak is significantly reduced at higher IPA concentrations (more evident in number density RDFs, **Figure S1**), suggesting that the solvation shell of water is disrupted at longer distances due to IPA (number density of IPA increases at these distances). At higher solute concentration (w_A= 0.5), the water RDFs display peak intensities comparable to those in the dilute case at similar solvent compositions, indicating that the relative enrichment of water in the solvation shell is maintained. However, the absolute number of available water molecules per solute is reduced, as reflected in the number density RDFs (**Figure S1**), consistent with increased competition among solute molecules for available water. Nevertheless, the first peak at w_I=0 is sharper than in the dilute case, while at w_I=0.2, within the LLPS regime, the third peak becomes relatively more pronounced, suggesting a reorganization of the extended hydration structure under phase-separating conditions.

In contrast, as shown in **Figure 2c** and **d**, RDFs of IPA molecules show markedly weaker coordination with BAL. The first discernible peak occurs at ~0.42 nm, outside the primary hydration shell, with a much lower intensity than that of water. Moreover, at lower solute concentrations, IPA shows almost no preferential association with the solute, whereas at higher solute concentrations, RDFs fluctuate irregularly, reflecting disordered, heterogeneous interactions in the crowded environment. This suggests that IPA molecules are largely excluded from direct solute-solvent interactions, occupying more diffuse positions in or after the second solvation shell. At low IPA concentrations, the RDF peak is broad, reflecting weak, nonspecific interactions. This indicates that IPA molecules become increasingly associated with BAL surfaces, not by direct hydrogen bonding, but by filling voids created as water structure weakens. To quantify this disruption, we calculated the mean H-bond degree, ⟨k⟩ (the average number of hydrogen bonds per water molecule in the solvation shell; see Section S2 for details). At a lower solute concentration (w_A = 0.15), ⟨k⟩ decreases monotonically with increasing IPA fraction. Conversely, at a higher solute concentration (w_A = 0.5), the hydrogen bond network exhibits an initial slight increase, indicative of localized water clustering, before undergoing a sharp decline at higher antisolvent fractions (**Figure S3**), underscoring its role as a destabilizer of water structuring rather than as a direct competitive binder.

View Article Online
DOI: 10.1039/D6CP00296J

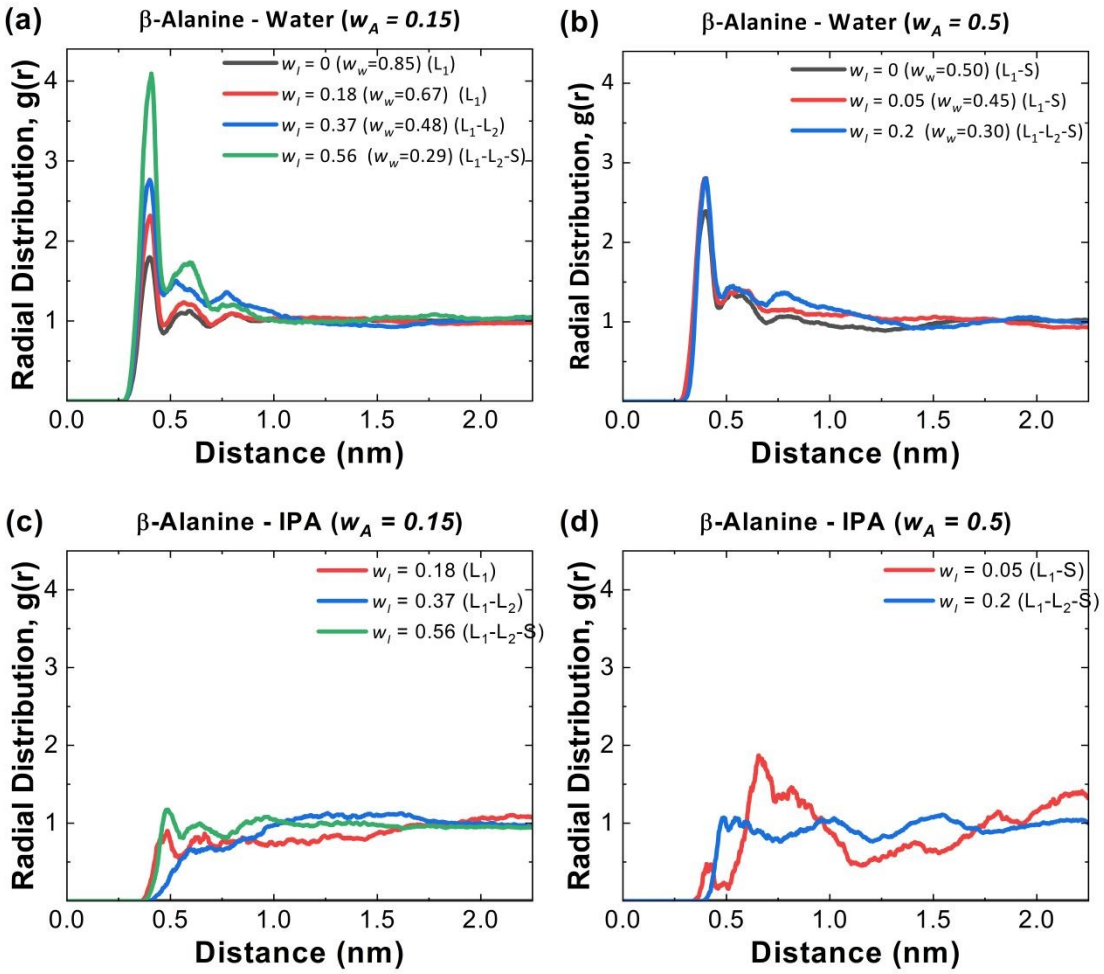

Figure 2: Radial Distribution of water and IPA around BAL at two different weight fractions $\boldsymbol{w_A}$=0.15 and $\boldsymbol{w_A}$=0.5. (a) RDF of water around BAL at $\boldsymbol{w_A}$=0.15 (b) RDF of water around BAL at $\boldsymbol{w_A}$=0.5 (c) RDF of IPA around BAL at $\boldsymbol{w_A}$=0.15 (d) RDF of IPA around BAL at $\boldsymbol{w_A}$=0.5. The legend denotes the weight fraction of the antisolvent IPA ($\boldsymbol{w_I}$) and water ($\boldsymbol{w_w}$).

Together, these results show that water overwhelmingly governs the solvation shell of BAL, while IPA exerts its effect indirectly, by eroding the structural integrity of extended hydration networks. The collapse of oscillatory water RDFs beyond the first shell is particularly diagnostic of the approach to LLPS, as compared to water RDF behavior in our previous work on antisolvent crystallization, signaling the breakdown of long-range solvent ordering.[22] IPA, while weakly coordinated, enhances this disruption by promoting heterogeneous solvent environments. Thus, the transition toward oiling-out is not marked by replacement of water by IPA, but by progressive weakening of water structuring, partial desolvation of β-alanine, and enhanced clustering of solute molecules. These microscopic events foreshadow the formation of solute-rich droplets characteristic of the oiling-out transition. These trends are quantitatively confirmed by the average coordination numbers reported in **Table S2,** which shows a decrease

View Article Online
DOI: 10.1039/D6CP00296J

in water occupancy, while IPA coordination remains comparatively low, indicating incomplete compensation of the solvation shell.

The three-dimensional spatial distribution functions (SDFs) further highlight how the solvent environment reorganizes around BAL. At low IPA mole fractions in the non-LLPS region, the SDFs show a dense and continuous water envelope surrounding both the carboxylate and amine groups of BAL (**Figure 3a**,**b**,**e**,**f**). This hydrogen-bonded hydration shell provides strong stabilization, with local water density exceeding the bulk value by a significant margin. IPA molecules are almost entirely excluded from this first shell, appearing only as weak, diffuse density clouds farther from the solute. This observation is consistent with the RDF analysis and reinforces that water dominates the primary solvation environment at low IPA content. As IPA concentration increases, the water coverage begins to fragment, and patches of IPA density emerge in regions previously occupied by water (**Figure 3c**,**d**,**g**). This change is especially evident near the amine group, where IPA oxygen atoms intrude into the hydration zone but fail to establish the strong directional hydrogen bonds that characterize water-solute interactions. Instead, the IPA isosurfaces appear disordered and dispersed, suggesting transient association rather than stable solvation. The result is a heterogeneous shell in which water molecules no longer form a continuous hydrogen-bond network, and IPA molecules occupy only partial, weakly bound positions. Such mixed coverage reflects competition between water and IPA, but it reveals that IPA cannot replicate water's stabilizing role. Crucially, IPA fails to compensate for the enthalpic stabilization lost by water, resulting in a partially desolvated state. The resulting 'solvation voids' expose the BAL surface, creating high-energy patches that drive solute-solute association to minimize surface free energy.

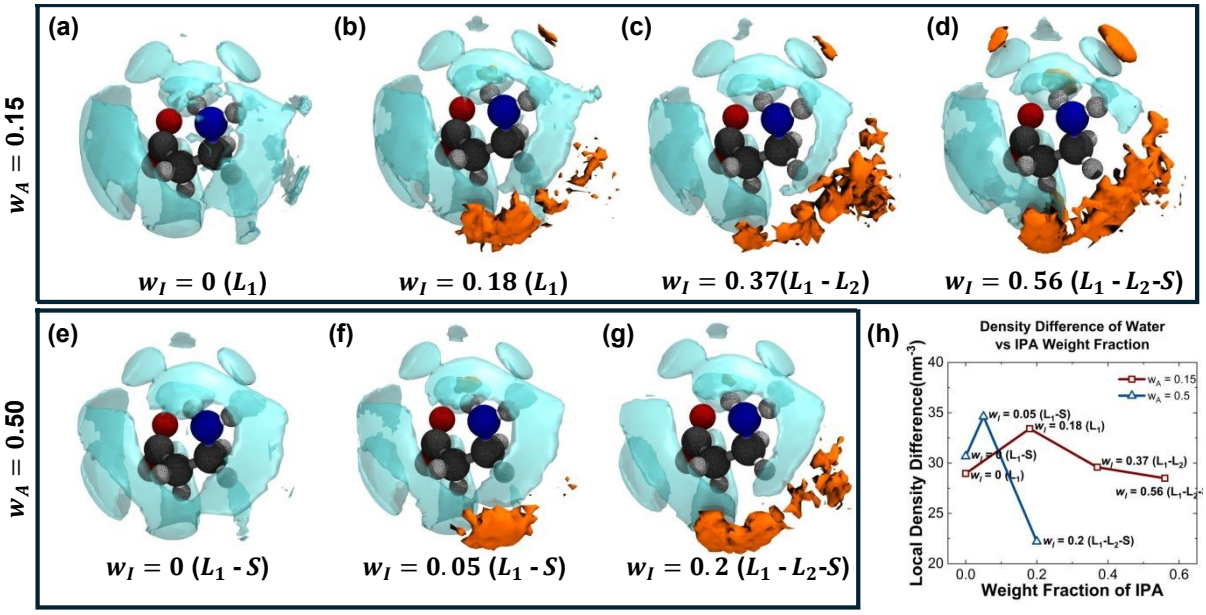

View Article Online
DOI: 10.1039/D6CP00296J

Figure 3: Spatial distribution of water (blue) and IPA (orange) around BAL at two solute weight fractions, $\boldsymbol{w_A}$ = 0.15 (a-d) and $\boldsymbol{w_A}$ = 0.5 (e-g), across different IPA weight fractions. (h) Local density difference of water relative to bulk as a function of IPA composition at different weight fractions of BAL.

Upon crossing into the LLPS regime, the disruption of hydration becomes stark. Water density around BAL isosurfaces becomes discontinuous and patchy (**Figure 3f**, **g**), marking the rupture of the solvation shell. IPA density increases near the solute surface, but the distributions remain diffuse and lack the distinct coordination patterns characteristic of water. This incomplete compensation indicates that BAL molecules in droplets are partially desolvated, with solvent structuring insufficient to shield solutes from one another. Such conditions favor enhanced solute-solute contacts, thereby promoting clustering towards a dense state followed by nucleation. SDF isosurfaces were visualized at the first solvation shell level, as including the second and third shells would result in clustering and make them difficult to distinguish in three-dimensional representations. The disruption of extended hydration structure beyond the first shell is instead captured by the diminished second and third peaks in the RDFs (**Figure 2**).

The consequences of this solvent restructuring are quantified by subtracting the bulk density from the peak number density values of water in the solvation shell (termed as local density difference) and are displayed in Figure 3h. While coordination numbers provide the absolute number of solvent molecules, this relative measure captures the extent of preferential hydration. As the bulk water density decreases with increasing IPA addition, the local density difference indicates whether water continues to cluster around the BAL surface, independent of the changing bulk composition. In both solute-rich and lean regimes, the initial addition of IPA triggers an increase in the local water density difference relative to bulk. As the bulk solution becomes slightly IPA-rich, water molecules are energetically driven to cluster around the hydrophilic BAL to minimize its contact with the antisolvent. This creates a locally enriched hydration shell that is significantly denser than the increasingly IPA-rich bulk mixture (w_I=0 vs w_I =0.05), effectively shielding the solute in the single-phase liquid region. As IPA concentration increases further, entering the LLPS regime, this protective mechanism fails, leading to a drop in local water density. In the LLPS regime, the bulk IPA concentration is high enough to disrupt the hydrogen-bond network sustaining the enriched shell. Water molecules are stripped away faster than they can be recruited, without being replaced by IPA (as observed in the SDFs). The local density data quantitatively distinguish two regimes of antisolvent action. In a solute-lean phase (at w_A=0.15, w_I=0.18), IPA promotes water enrichment around the solute (stabilization). However, in a solute-rich phase (at w_A=0.50, w_I=0.2), it forces the ejection of water without replacement (destabilization), directly correlating with the formation of solute-rich droplets. This can also be seen in Figure S1, where at w_I= 0.18, the bulk water density is reduced relative to w_I= 0 owing to the presence of IPA, yet the first solvation shell around BAL retains a comparable absolute water density. Direct comparison of g(r) peak heights between the two compositions, therefore, understates the magnitude of the local water enrichment. Together, the SDF and

View Article Online
DOI: 10.1039/D6CP00296J

density-difference analyses reveal that during oiling-out crystallization, β-alanine molecules lose stabilizing water coverage and transition into a partially desolvated state within solute-rich droplets. This state weakens solute-solvent interactions and promotes solute-solute association, offering a direct molecular mechanism for a pathway toward nucleation and crystal growth.

To better understand solute–solute association, β-alanine–β-alanine radial distribution functions were computed for fully solvated (FS) and partially desolvated (PS) states at each composition (Figure S2). At the dilute BAL concentration (w_A = 0.15; **Figure S2a,c**), the first peak at ~0.45 nm in the fully solvated state is lowest at w_I = 0 (~1.8) rises to ~3.4 at w_I = 0.18 and ~4.1 at w_I = 0.37, and sits at ~2.8 at w_I = 0.56. In the partially desolvated state, the first peak rises monotonically with IPA content from ~2.8 at w_I= 0 to ~6.2 at w_I= 0.56, the strong-LLPS composition; the increase as β-alanine transitions from fully solvated to partially desolvated is therefore largest at w_I = 0.56. This provides direct molecular evidence that, in the strong-LLPS regime, β-alanine actively clusters as its hydration shell is stripped away. At w_I = 0.5 (**Figure S2b,d**), the amplitudes are lower overall because frequent β-alanine contacts occur even in the fully solvated state: the fully solvated first peak sits near ~1.8, ~1.7, and ~2.0 for w_I = 0, 0.05, and 0.2, while the partially desolvated peak is essentially unchanged at ~1.7 and ~1.75 for w_I = 0 and 0.05 but rises to ~2.4 at the LLPS composition w_I = 0.2, reinforcing the pattern seen at w_A = 0.15, desolvation promotes clustering, and the effect is strongest at the composition within each series at which LLPS is observed. A structured second peak at ~0.55 nm that sharpens with IPA content and is most prominent in the partially desolvated state is consistent with the emergence of preferred intermolecular spacings that precede nucleation, supporting the picture of solute-rich aggregates as precursors to nucleation consistent with the oiling-out pathway.

The functional-group-specific RDFs of water (**Figure 4a**-**c**) reveal distinct hydration preferences that evolve with composition and confirm that hydration is not evenly distributed between the two termini of BAL. Around the -COO^- group, a sharp first peak at ~0.23 nm reflects strong hydrogen bonding with water, and multiple secondary peaks extend to ~0.7 nm, indicating long-range layering stabilized by electrostatic interactions. In contrast, the -NH_3^+ group exhibits a first-shell peak at approximately 0.20 nm, albeit with lower intensity and pronounced secondary oscillations, indicating weaker hydration compared to the carboxylate group. These differences suggest that the -COO^- group anchors a structured hydration network, whereas the -NH_3^+ group is more easily destabilized. As IPA content decreases, the intensity of the first peaks decreases for both groups, and the multiple peaks in the -COO^- RDF broaden and diminish, signaling loss of extended structuring. The amine RDF collapses even more rapidly, reflecting an earlier onset of desolvation around this group.

Overall, the solvation environment of BAL can be separated into fully solvated and partially desolvated states. In the fully solvated state, the hydration shell is intact, with water

View Article Online
DOI: 10.1039/D6CP00296J

molecules continuously occupying the first coordination zone around both the carboxylate (-COO^-) and amine (-NH_3^+) groups. In the partially desolvated state, portions of the shell are vacated, especially when the solute molecules interact with each other, leaving BAL exposed and more prone to intermolecular association with fewer solvent molecules around it. These two states represent distinct stages of solvation breakdown, and their comparison provides molecular-level insight into the progression from homogeneous solution to heterogeneous solution.

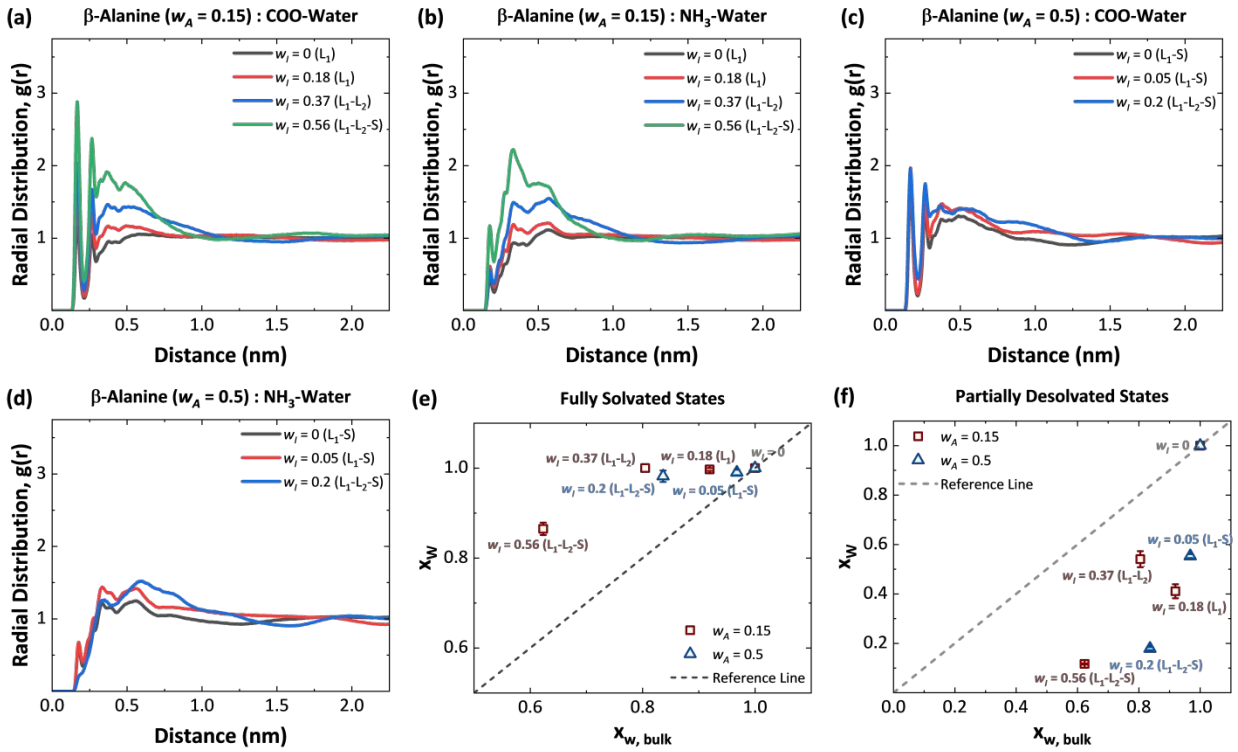

Figure 4: Radial distribution functions of water around BAL for the carboxylate (a,c), and amine (b,d) functional groups at two different weight fractions of BAL: 0.15 (a,b), 0.5 (c,d). Water mole fractions (in solvent-antisolvent mixture) in the solvation shell compared to bulk are shown for fully solvated (e) and partially desolvated (f) states. All subfigures in the panel are plotted at different IPA weight fractions as shown in the legend.

The composition of both solvents in the solvation shell relative to the bulk reveals a sharper distinction between solvation states (**Figure 4e**, **f**). In the fully solvated state (**Figure 4e**), the water mole fraction (of water-IPA mixture) in the shell is consistently above the reference line for all IPA-containing mixtures, showing persistent preferential hydration of BAL even as the bulk becomes increasingly IPA-rich. The only exception is the pure-water case (w_I=0), which naturally lies on the line since solvation shell and bulk are equal to a mole fraction of 1. More importantly, as the IPA concentrations are very high, the water concentrations inside the solvation shell are farther from the reference line, suggesting that the IPA drives enrichment of

View Article Online
DOI: 10.1039/D6CP00296J

water inside the shell. This result highlights that as long as the hydration shell remains intact, BAL maintains a bias toward water-rich local environments relative to the surrounding liquid. In contrast, in the partially desolvated state (**Figure 4f**), all data points except the pure-water case fall below the reference line, indicating that the hydration shell becomes water-depleted relative to bulk once desolvation sets in.

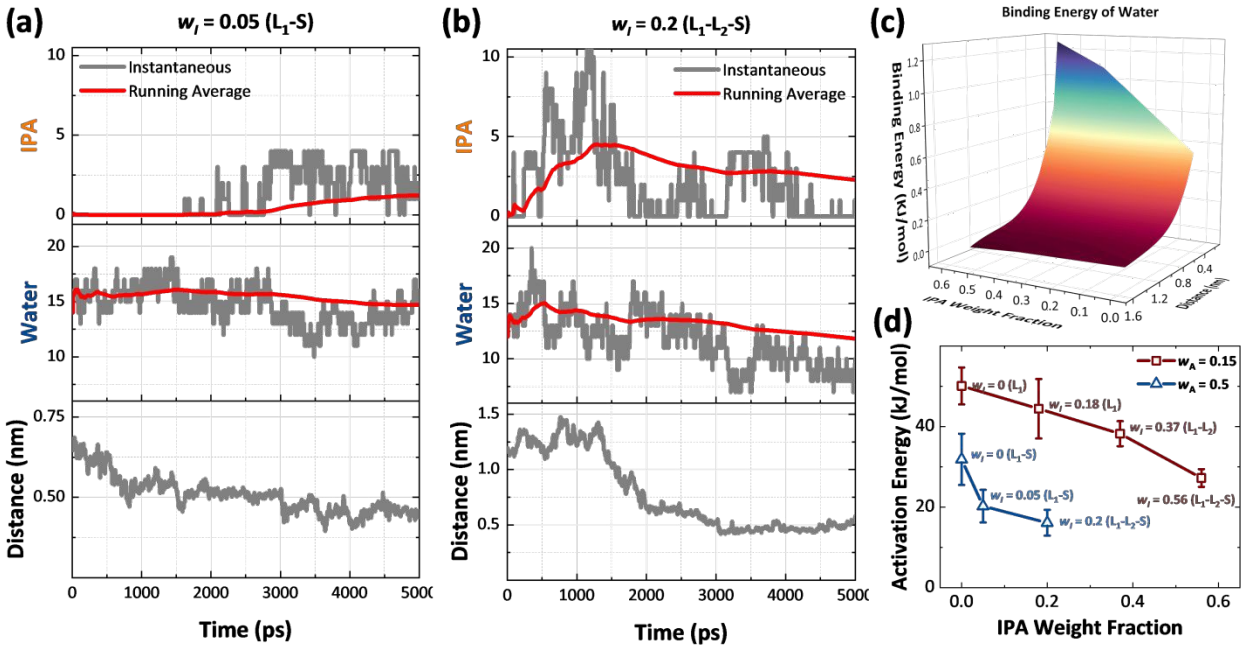

Figure 5: Time evolution of solvent coordination numbers and solute–solute distance for β-alanine at w_A= 0.5, comparing (a) non-LLPS (w_I= 0.05), and (b) LLPS (w_I= 0.2) conditions. (c) Binding energy of water molecules calculated using the MM-PBSA method across solvent compositions. (d) Activation energies for the transition from fully solvated to partially desolvated states obtained from the double-well potential method.

The energetic signature of this transition is quantified by the activation barriers calculated with the double-well potential method (**Figure 5d**). Details of the double-well potential method are provided in **Section S2** of the supporting information. The barrier associated with moving from the fully solvated to the partially desolvated state decreases systematically with increasing IPA content, reaching its lowest values in the LLPS regime. This trend demonstrates that desolvation becomes progressively easier in IPA-rich environments, reflecting the destabilization of hydration networks. Additionally, as BAL concentrations increase, the activation barrier decreases further, suggesting easier crystal nucleation. At comparable IPA weight fractions (w_I = 0.18 at w_A = 0.15, and w_I = 0.20 at w_A = 0.50), the activation energy is substantially smaller at wA = 0.50. We attribute this to the higher solute concentration, which increases crowding and further destabilizes the solvation shell. Thus, the driving force for oiling-out is not enhanced IPA-

View Article Online
DOI: 10.1039/D6CP00296J

solute attraction, but the limited favorable water-solute interactions that leave BAL incompletely solvated. These results demonstrate that the onset of oiling-out crystallization is facilitated by both the synchronous depletion of water and IPA in LLPS conditions and by a progressive lowering of the desolvation barrier. In droplets, this instability produces partially desolvated BAL molecules that readily cluster, completing the molecular mechanism linking hydration collapse to nucleation. The intrinsic enthalpic favorability of β-alanine self-association is further supported by gas-phase DFT studies demonstrating that β-alanine dimers and higher-order oligomers are stabilized by strong O–H···N hydrogen bonds, with dissociation energies increasing systematically with cluster size through cooperative ring interactions.[26] This is consistent with the solute clustering behavior observed in our trajectories and supports the mechanistic picture of partially desolvated molecules aggregating into a disordered dense phase prior to lattice integration.

To quantify the energetic cost of desolvation, an extended double-well potential approach was used to construct energy profiles along a crystallization coordinate (**Figure 6a**, **b**)[22,23]. First, potential energy profiles were generated for the fully solvated and partially desolvated states of BAL. The partially desolvated profile was shifted by the binding energy required to remove the excess solvent molecules, calculated using the MM-PBSA method. Per-composition means and standard deviations across the six sampled frames are reported in **Table S3**.[27] The activation energy was defined as the difference between the minimum energy of the fully solvated state and the intersection point of the two energy profiles, which marks the transition state for desolvation (**Figure S4**). To capture the subsequent evolution of the partially desolvated state, the molecular configuration at this intersection state was systematically rotated through all possible orientations, and the lowest-energy configuration was identified. The orientational dependence of the potential energy is quantified by the rotational energy landscape (**Figure S5**), which shows that the energy varies with molecular orientation. This confirms that orientational selection is an energetic requirement for lattice integration. From the lowest-energy orientation, a new potential energy profile was generated, corresponding to the reorganization step along the crystallization pathway.

In this way, three energy profiles were plotted together: the initial fully solvated state, the transition through the partially desolvated state, and the final rotated minimum that represents the configuration predisposed to solute-solute association. The crystallization coordinate (x-axis in **Figure 6**) was defined such that the fully solvated minimum lies at zero, while the partially desolvated and rotated minima appear at progressively higher values. These profiles collectively describe the multi-step energetic pathway by which BAL molecules transition from hydration-stabilized states in a homogeneous solution through a desolvated transition state, dense state, and fully desolvated state to a crystal lattice. The resulting landscapes reveal two distinct activation barriers that govern the kinetics of phase separation and ordering. The first barrier, located at a crystal coordinate of 0.3, corresponds to the enthalpic penalty of stripping

View Article Online
DOI: 10.1039/D6CP00296J

the tightly bound hydration shell to access the partially desolvated state. The downhill progression in energy leads to a dense state, where the molecules require reorientation. The second barrier, located at a crystal coordinate of 0.7, represents the energetic cost of structural reorganization and rotational alignment required for dense clusters to form fully desolvated clusters. Finally, the second energy downhill represents the formation of crystal lattice or integration into an existing one. Additionally, when these energy costs are converted to probabilities of forming a dense state and crystalline state, the nature of the final product formed can be easily visualized, as depicted in **Figure 6c**. Details regarding the calculation of these probabilities are provided in Section 3 of the Supporting Information.

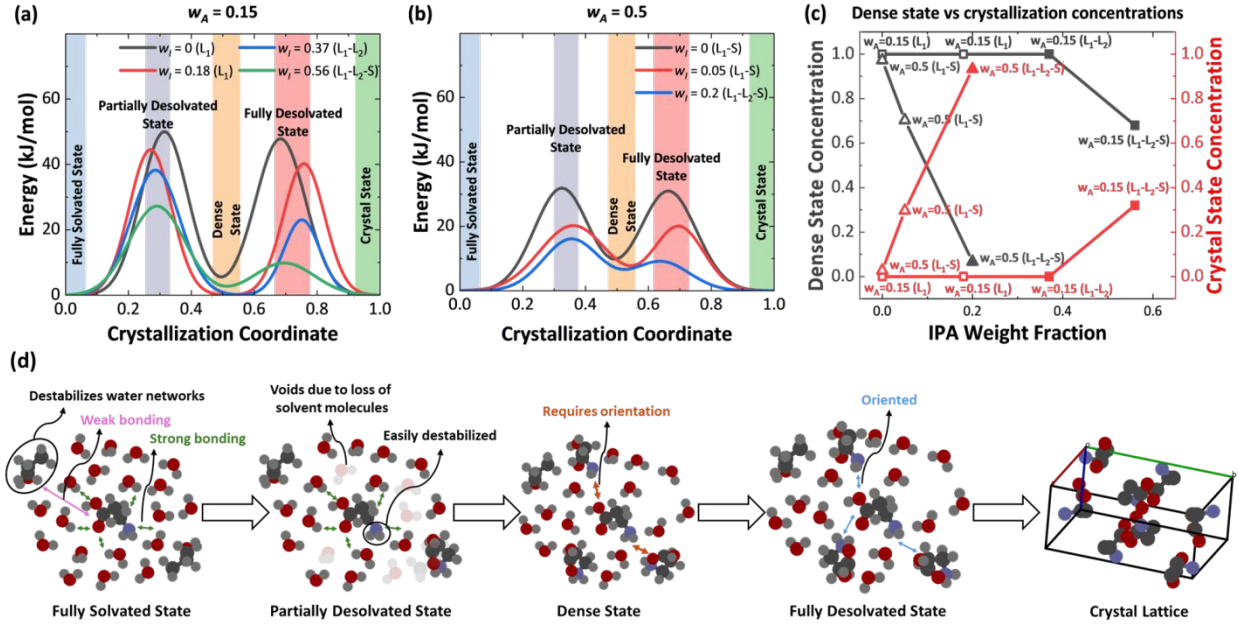

Figure 6: Energy profiles governing the transition from fully solvated states to crystal lattice for BAL-water-IPA solutions at solute weight fractions (a) w_A = 0.15 and (b) w_A = 0.5. IPA weight fractions are provided in the legend. (c) Probability of forming a dense state versus crystallization calculated from the energy profiles. Squares and triangles represent a solute weight fraction of 0.15 and 0.5, respectively, while the filled data points represent the oiling-out regions. Grey colored points correspond to dense state probability, while the red colored ones represent crystallization probability. (d) Molecular mechanism of solvent-mediated destabilization driving oiling-out crystallization. In the fully solvated state, BAL is stabilized by a robust hydration shell. IPA interacts weakly with the solute but disrupts the surrounding bulk water network. As the hydration shell fractures, water molecules are stripped away without being replaced by IPA in the partially desolvated state, creating high-energy solvation voids, particularly around the destabilized amine group. To minimize the free energy of these exposed surfaces, the molecules aggregate and undergo rotational reorientation during the dense state, forming a fully desolvated state. Finally, after complete aggregation and orientation, solute molecules form a crystal lattice or join the already existing one. Atom colors: oxygen (red), hydrogen (white), carbon (grey), nitrogen (purple).

In the dilute regime (w_A = 0.15, **Figure 6a**), the system in pure water (black line) exhibits substantial barriers for both desolvation (~50 kJ/mol) and reorganization. These high penalties

View Article Online
DOI: 10.1039/D6CP00296J

kinetically trap the solute in the solvated or dense state, preventing nucleation. The same can be observed at increased IPA concentrations (w_I = 0.18 – L_1 regime, w_I = 0.37-LLPS regime), as shown in **Figure 6c.** Hence, the probability of being in a dense state is significantly higher. However, further addition of IPA dramatically reshapes this landscape. As the IPA fraction increases to w_I = 0.56 (green line, **Figure 6a**), composition within the experimental LLPS region, the first barrier effectively collapses (<30 kJ/mol), and the second barrier is markedly reduced. This indicates that in the oiling-out regime, the solvent environment destabilizes the hydration shell, allowing the system to spontaneously access the dense liquid precursor state (70% probability, **Figure 6c**) followed by lattice integration (30% probability, **Figure 6c**).

At higher solute loading (w_A = 0.5, **Figure 6b**), the energy landscapes reveal the synergistic effect of solute crowding and antisolvent addition. Notably, in pure water, the barrier is lower compared to the dilute case (~30 kJ/mol vs ~ 50 kJ/mol). Since the supersaturation value is very low, the crystallization probability is much lower (~3%, **Figure 6c**). However, this barrier reduction explains the experimental observation of crystallization in the pure aqueous system. The frequent solute-solute collisions in the crowded environment statistically facilitate overcoming the desolvation and reorganization penalties. It should be noted that even a small increase in IPA concentration (w_I = 0.05), the crystallization probability increased to ~30% (**Figure 6c**). Moreover, the transition to the oiling-out regime (w_I = 0.2, blue line in **Figure 6b**) is marked by a further lowering of both barriers. The presence of IPA at this concentration minimizes the desolvation cost (peak 1) while simultaneously reducing the reorganization penalty (peak 2). This dual reduction implies that the oiled-out droplets are not merely amorphous aggregates but kinetically favored intermediates in which the energetic costs of both solvent removal and reorientation for lattice integration are significantly reduced. These results provide a quantitative energetic rationale for the oiling-out phenomenon, confirming that LLPS facilitates crystallization by reducing the kinetic resistance to both desolvation and structural ordering.

The overall molecular pathway driving oiling-out crystallization is summarized in **Figure 6d**. In the fully solvated state, BAL is stabilized by a robust hydration shell characterized by strong solute-water bonding, while the antisolvent (IPA) interacts only weakly and non-specifically with the surface. The onset of phase separation is triggered when the antisolvent destabilizes this network, not by competitive binding, but by forcing the ejection of water molecules without replacement. This creates a partially desolvated state defined by high-energy solvation voids where solvent shielding is lost, particularly around the easily destabilized amine groups. These voids lower the energetic penalty for aggregation, allowing the system to access a kinetically favored dense liquid state followed by a reorganization into a fully desolvated state. Molecules at the fully desolvated state then integrate into existing crystal lattices or form a new one.

View Article Online
DOI: 10.1039/D6CP00296J

Conclusions

In this study, we have established a molecular-level framework for understanding oiling-out crystallization post-LLPS, using the β-alanine (BAL)-water-IPA system as a model to link solvation structure to nucleation energetics and, thereby, kinetics. By integrating static structural analysis with dynamic free energy profiling, we identified the microscopic sequence of events that lead to crystallization. First, our structural analysis utilizing radial and spatial distribution functions demonstrates that the onset of LLPS is governed by the destabilization of the primary hydration shell. We found that IPA acts indirectly; it does not competitively displace water but rather fragments the hydrogen-bonded network that stabilizes the solute. This fragmentation results in a unique partially desolvated state characterized by solvation voids -surface patches where water is depleted and IPA interactions are too diffuse to provide stabilization. Second, we quantified the energetic consequences of this structural breakdown. The energy landscapes constructed along the crystallization coordinate revealed that nucleation is mediated by two distinct barriers: a desolvation barrier (stripping the hydration shell) and a reorganization barrier (orienting for lattice integration). In water-rich homogeneous solutions, the high energetic cost of desolvation kinetically traps the solute (at lower concentrations). However, within the LLPS regime, the compromised solvation environment systematically lowers these barriers.

Finally, these results provide strong computational support for the two-step nucleation theory in small-molecule systems. Our data show that the dense liquid droplets formed during oiling-out are not merely thermodynamic byproducts but are active, low-energy kinetic intermediates. By bypassing the high-energy pathway of direct nucleation from solution, these droplets facilitate crystallization by pre-paying the energetic cost of desolvation and crowding. This mechanistic insight suggests that process design strategies should view oiling-out not solely as a hindrance, but as a tunable state where manipulating the solvent/antisolvent ratio can precisely control the activation barriers for nucleation and growth.

Author contributions

P.K.R.: Conceptualization, Methodology, Software, Formal analysis, Investigation, Data curation, Writing– original draft. A.I.: Software, Formal analysis, Investigation, Data curation, Writing– revised draft. M.R.S.: Conceptualization, Resources, Supervision, Writing– review & editing

Conflicts of Interest

The authors declare that there are no conflicts of interest.

Data Availability

The data supporting this article have been included as part of the Supplementary Information. Supplementary information: number density radial distribution functions of water and IPA

View Article Online
DOI: 10.1039/D6CP00296J

around β-alanine (Figure S1); β-alanine–β-alanine radial distribution functions for fully solvated and partially desolvated states (Figure S2); MM-PBSA binding energy analysis (Figure S3); double-well potential construction (Figure S4); rotational energy landscapes (Figure S5); time evolution of coordination numbers, intermolecular distances, and hydrogen-bond network statistics (Figure S6); time-block RDF analysis (Figure S7); simulated system compositions and molecular counts (Table S1); coordination numbers within the first solvation shell (Table S2); and per-molecule binding energies of water (Table S3). Additional simulation input files, analysis scripts, and raw trajectory data are available from the corresponding author upon reasonable request.

Acknowledgments

This material is based on the work performed at the Materials and Systems Engineering Laboratory at the University of Illinois Chicago (UIC). M.R.S. acknowledges funding support from UIC, and the US National Science Foundation (NSF) grants - EFRI 2132022, and CMMI 2326714.

References

(1) Meng, Z.; Huang, Y.; Cheng, S.; Wang, J. Investigation of Oiling-Out Phenomenon of Small Organic Molecules in Crystallization Processes: A Review. *ChemistrySelect* **2020**, *5* (26), 7855-7866.
(2) Tanaka, K.; Takiyama, H. Effect of Solution Composition on Impurity Profile of the Crystallized Product in Oiling-Out Crystallization. *Chemical and Pharmaceutical Bulletin* **2020**, *68* (4), 326-331.
(3) Zhang, T. H.; Liu, X. Y. How does a transient amorphous precursor template crystallization. *Journal of the American Chemical Society* **2007**, *129* (44), 13520-13526.
(4) Myerson, A. S. *Handbook of Industrial Crystallization*; 2002.
(5) Sun, M.; Tang, W.; Du, S.; Zhang, Y.; Fu, X.; Gong, J. Understanding the roles of oiling-out on crystallization of β-alanine: unusual behavior in metastable zone width and surface nucleation during growth stage. *Crystal Growth & Design* **2018**, *18* (11), 6885-6890.
(6) Coliaie, P.; Prajapati, A.; Ali, R.; Boukerche, M.; Korde, A.; Kelkar, M. S.; Nere, N. K.; Singh, M. R. In-line measurement of liquid–liquid phase separation boundaries using a turbidity-sensor-integrated continuous-flow microfluidic device. *Lab on a Chip* **2022**, *22* (12), 2299-2306.
(7) Sun, M.; Du, S.; Chen, M.; Rohani, S.; Zhang, H.; Liu, Y.; Sun, P.; Wang, Y.; Shi, P.; Xu, S. Oiling-out investigation and morphology control of β-alanine based on ternary phase diagrams. *Crystal Growth & Design* **2018**, *18* (2), 818-826.
(8) Cinar, H.; Fetahaj, Z.; Cinar, S.; Vernon, R. M.; Chan, H. S.; Winter, R. H. Temperature, hydrostatic pressure, and osmolyte effects on liquid–liquid phase separation in protein condensates: physical chemistry and biological implications. *Chemistry–A European Journal* **2019**, *25* (57), 13049-13069.
(9) Sanadhya, S.; Tucker, Z. D.; Gulotty, E. M.; Boggess, W.; Ashfeld, B. L.; Moghaddam, S. Thermodynamic descriptors of sensible heat driven liquid-liquid phase separation. *Journal of Molecular Liquids* **2022**, *360*, 119440.

View Article Online
DOI: 10.1039/D6CP00296J

(10) Pezzotti, S.; König, B.; Ramos, S.; Schwaab, G.; Havenith, M. Liquid–liquid phase separation? Ask the water! *The Journal of Physical Chemistry Letters* **2023**, *14* (6), 1556-1563.
(11) Gao, Z.; Altimimi, F.; Gong, J.; Bao, Y.; Wang, J.; Rohani, S. Ultrasonic irradiation and seeding to prevent metastable liquid–liquid phase separation and intensify crystallization. *Crystal Growth & Design* **2018**, *18* (4), 2628-2635.
(12) Zhao, H.; Xie, C.; Xu, Z.; Wang, Y.; Bian, L.; Chen, Z.; Hao, H. Solution crystallization of vanillin in the presence of a liquid–liquid phase separation. *Industrial & engineering chemistry research* **2012**, *51* (45), 14646-14652.
(13) Huang, Y.; Wang, J.; Wang, N.; Li, X.; Ji, X.; Yang, J.; Zhou, L.; Wang, T.; Huang, X.; Hao, H. Molecular mechanism of liquid–liquid phase separation in preparation process of crystalline materials. *Chemical Engineering Science* **2022**, *262*, 118005.
(14) Wolde, P. R. t.; Frenkel, D. Enhancement of protein crystal nucleation by critical density fluctuations. *Science* **1997**, *277* (5334), 1975-1978.
(15) Erdemir, D.; Lee, A. Y.; Myerson, A. S. Nucleation of crystals from solution: classical and two-step models. *Accounts of chemical research* **2009**, *42* (5), 621-629.
(16) Sosso, G. C.; Chen, J.; Cox, S. J.; Fitzner, M.; Pedevilla, P.; Zen, A.; Michaelides, A. Crystal Nucleation in Liquids: Open Questions and Future Challenges in Molecular Dynamics Simulations. *Chemical Reviews* **2016**, *116* (12), 7078-7116. DOI: 10.1021/acs.chemrev.5b00744.
(17) Torrie, G. M.; Valleau, J. P. Nonphysical sampling distributions in Monte Carlo free-energy estimation: Umbrella sampling. *Journal of computational physics* **1977**, *23* (2), 187-199.
(18) Duan, X.; Wei, C.; Liu, Y.; Pei, C. A molecular dynamics simulation of solvent effects on the crystal morphology of HMX. *Journal of hazardous materials* **2010**, *174* (1-3), 175-180.
(19) Finney, A. R.; Salvalaglio, M. Molecular simulation approaches to study crystal nucleation from solutions: Theoretical considerations and computational challenges. *Wiley Interdisciplinary Reviews: Computational Molecular Science* **2024**, *14* (1), e1697.
(20) Dighe, A. V.; Coliaie, P.; Podupu, P. K.; Singh, M. R. Selective desolvation in two-step nucleation mechanism steers crystal structure formation. *Nanoscale* **2022**, *14* (5), 1723-1732.
(21) Dighe, A. V.; Podupu, P. K.; Singh, M. R. Emulsification of Supersaturated Solutions Amplifies Induction Time Variation in Crystallization. *Crystal Growth & Design* **2023**, *23* (9), 6290-6297.
(22) Dighe, A. V.; Podupu, P. K. R.; Coliaie, P.; Singh, M. R. Three-Step Mechanism of Antisolvent Crystallization. *Crystal Growth & Design* **2022**, *22* (5), 3119-3127. DOI: 10.1021/acs.cgd.2c00014.
(23) Dighe, A. V.; Singh, M. R. Solvent fluctuations in the solvation shell determine the activation barrier for crystal growth rates. *Proc. Natl. Acad. Sci. U. S. A.* **2019**, *116*, 23954.
(24) Abraham, M. J. GROMACS: High performance molecular simulations through multi-level parallelism from laptops to supercomputers. *SoftwareX* **2015**, *1–2*, 19.
(25) Brehm, M.; Thomas, M.; Gehrke, S.; Kirchner, B. TRAVIS—A free analyzer for trajectories from molecular simulation. *The Journal of Chemical Physics* **2020**, *152* (16). DOI: 10.1063/5.0005078 (acccessed 10/3/2025).
(26) Piekarski, D. G.; Díaz-Tendero, S. Structure and stability of clusters of β-alanine in the gas phase: importance of the nature of intermolecular interactions. *Physical Chemistry Chemical Physics* **2017**, *19* (7), 5465-5476, 10.1039/C6CP07792G. DOI: 10.1039/C6CP07792G.
(27) Kumari, R.; Kumar, R.; Consortium, O. S. D. D.; Lynn, A. g_mmpbsa- A GROMACS tool for high-throughput MM-PBSA calculations. *Journal of chemical information and modeling* **2014**, *54* (7), 1951-1962.

View Article Online
DOI: 10.1039/D6CP00296J

The data supporting this article have been included as part of the Supplementary Information. Supplementary information: number density radial distribution functions of water and IPA around β-alanine (Figure S1); β-alanine–β-alanine radial distribution functions for fully solvated and partially desolvated states (Figure S2); MM-PBSA binding energy analysis (Figure S3); double-well potential construction (Figure S4); rotational energy landscapes (Figure S5); time evolution of coordination numbers, intermolecular distances, and hydrogen-bond network statistics (Figure S6); time-block RDF analysis (Figure S7); simulated system compositions and molecular counts (Table S1); coordination numbers within the first solvation shell (Table S2); and per-molecule binding energies of water (Table S3). Additional simulation input files, analysis scripts, and raw trajectory data are available from the corresponding author upon reasonable request.